A&A 497, 409–421 (2009)
DOI: 10.1051/0004-6361/200811018
© ESO 2009

Astronomy & Astrophysics

Long-wavelength observations of debris discs around sun-like stars⋆

V. Roccatagliata[1], Th. Henning[1], S. Wolf[2,1], J. Rodmann[3], S. Corder[4], J. M. Carpenter[4], M. R. Meyer[5], and D. Dowell[6]

[1] Max-Planck-Institut für Astronomie (MPIA), Königstuhl 17, 69117 Heidelberg, Germany
e-mail: roccata@mpia.de
[2] University of Kiel, Institute of Theoretical Physics and Astrophysics, Leibnizstrasse 15, 24098 Kiel, Germany
[3] Research and Scientific Support Department, ESA/ESTEC, 2201 AZ Noordwijk, The Netherlands
[4] California Institute of Technology, Department of Astronomy, MS 105-24, Pasadena, CA 91125, USA
[5] Steward Observatory, The University of Arizona, 933 North Cherry Avenue, Tucson, AZ 85721, USA
[6] Jet Propulsion Laboratory, California Institute of Technology, Mail Stop 169-506, Pasadena, CA 91109, USA

Received 23 September 2008 / Accepted 2 February 2009

ABSTRACT

Context. Tracing the evolution of debris discs is essential for our understanding of the architecture of planetary system. Even though the evolution of their inner discs has been recently studied with the Spitzer Space Telescope at mid- to far-infrared wavelengths, the outer discs are best characterised by sensitive millimetre observations.
Aims. The goal of our study is to understand the evolution timescale of circumstellar debris discs, and the physical mechanisms responsible for such evolution around solar-type stars. In addition, we make a detailed characterisation of the detected debris discs.
Methods. Two deep surveys of circumstellar discs around solar-type stars at different ages were carried out at 350 μm with the CSO and at 1.2 mm with the IRAM 30-m telescope. The dust disc masses were computed from the millimetre emission, where the discs are optically thin. Theoretically, the mass of the disc is expected to decrease with time. To test this hypothesis, we performed the generalised Kendall's tau correlation and three different two-sample tests. A characterisation of the detected debris discs has been obtained by computing the collision and Poynting-Robertson timescales and by modelling the spectral energy distribution.
Results. The Kendall's tau correlation yields a probability of 76% that the mass of debris discs and their age are correlated. Similarly, the three two-sample tests give a probability between 70 and 83% that younger and older debris systems belong to different parent populations in terms of dust mass. We detected submillimetre/millimetre emission from six debris discs, enabling a detailed SED modelling.
Conclusions. Our results on the correlation and evolution of dust mass as a function of age are conditioned by the sensitivity limit of our survey. Deeper millimetre observations are needed to confirm the evolution of debris material around solar-like stars. In the case of the detected discs, the comparison between collision and Poynting-Robertson timescales supports the hypothesis that these discs are dominated by collisions. All detected debris disc systems show the inner part evacuated from small micron-sized grains.

Key words. circumstellar matter – planetary systems: formation – stars: late-type – Kuiper Belt

1. Introduction

As part of the star formation process in molecular cloud cores, circumstellar discs form by conserving the initial angular momentum. These so-called *primordial* discs have typical masses (10^{-3}–10^{-2} $M_\odot$) and sizes comparable to what is expected for the primitive solar nebula, and they provide the environment and material from which planets are expected to form (Beckwith et al. 2000; Natta et al. 2007). The first stages of planet formation occur close to the disc mid-plane where submicron grains grow to millimetre sizes and settle (e.g. Beckwith et al. 2000). Larger planetesimals may successively form by collisions between grains and through gravitational instabilities (e.g. Johansen et al. 2007; Henning 2008). The primordial gas in circumstellar discs is thought to last for 1–10 Myr (e.g. Haisch et al. 2001; Lawson et al. 2004). After the gas is dispersed from the discs, the dust grains are removed from the optically thin disc by radiation pressure, Poynting-Robertson drag or dust sublimation on timescales shorter than the stellar pre-main sequence lifetime (Backman & Paresce 1993; Meyer et al. 2007). Nevertheless, an infrared excess above the stellar photosphere has been discovered around more than 300 pre- and main-sequence stars. These stars are thought to host a remnant *debris* disc. Backman & Paresce (1993) suggested that the infrared excess of these objects comes from small dust particles that are the products of collisions of larger bodies. Thus, a debris disc should consist of a "second generation" of small dust particles, larger bodies, and possibly, planets.

The formation of large bodies is thought to be faster in the inner part of the disc (Kenyon & Bromley 2004a). As a consequence, new small dust particles will be produced by collisions first in the inner region of the disc and, later, further out (Kenyon & Bromley 2004a). During this phase, small dust particles are continuously produced in the disc. In this perspective, *transitional objects* are of particular interest. These may represent a transitional phase between the primordial optically thick disc phase and the debris optically thin disc phase. Their infrared excess suggests the presence of an inner hole in the

⋆ This work is based on observations made with the IRAM (*Institut de Radioastonomie Millimétrique*) 30-m telescope and the CSO (*Caltech Submillimetre Observatory*) 10-m telescope. IRAM is supported by INSU/CNRS (France), MPG (Germany), and IGN (Spain).

disc where the small grain population, which emits in the near-IR, is missing. Some of them are still accreting material onto the central star, while others show intense collisional activity in their inner part, possibly induced by the formation of planets (Currie et al. 2007; Kenyon & Bromley 2004b).

While the dissipation of debris discs takes place by radiation pressure and/or Poynting-Robertson drag and the total dust mass decreases with time, at early stages the stellar wind drag can be an important dust removal mechanism. Depending on which of these processes is the main driver of dust removal, we expect a power-law dependence with a different index (Dominik & Decin 2003; Wyatt et al. 2007a,b; Löhne et al. 2008) and a different dust distribution if a planetesimal belt at a given distance is creating dust of just one size (Wyatt 2005). Spangler et al. (2001) measured the fractional luminosity ($L_{\rm IR}/L_{\rm star}$) of pre- and main sequence stars with ISO. They found that the fractional luminosity, which is proportional to the dust present in the disc, decreases with time as $t^{-1.76}$. While the analysis of Spangler et al. (2001) included also pre-main sequence stars, Habing et al. (2001) analysed the ISO and IRAS data of nearby main-sequence stars alone: they concluded that most of the stars reach the main-sequence surrounded by a disc which decays in about 400 Myr. Decin et al. (2003) reviewed the different studies on the time dependency of Vega-like systems done with ISO/IRAS. They concluded that the observations only indicated a large spread in fractional luminosity for stars at most ages, that the maximum excess was independent of time and that the debris disc phenomenon was more common in younger stars. An analysis of the near to far infrared excess, carried out with Spitzer, led to the finding of a general decrease of the fractional luminosity with time as t^{-1}, starting later at longer wavelengths (Su et al. 2006). This suggested a disc clearing more efficiently in the inner parts (Su et al. 2006). Deviations from these trends have been associated with a recent or still ongoing collisional cascade that produces a small dust grain population which is rapidly removed by radiation pressure or by the action of the Poynting-Robertson drag (Song et al. 2005; Wyatt et al. 2007b). A complementary picture of the evolution of the outer part of the debris discs is provided by (sub)millimetre observations. These show a decline in the dust mass as a function of age and significant evolution of the circumstellar dust mass within the first 10 Myr and between 10 Myr and a few Gyr (e.g. Liu et al. 2004; Carpenter et al. 2005, hereafter C05).

In this paper we present the results of two deep sub-millimetre and millimetre surveys of circumstellar discs around solar-type stars with ages between 3 Myr and 3 Gyr. The characteristics of our sample are presented in Sect. 2.1. The observations carried out at 350 μm and at 1.2 mm are reported in Sects. 2.2 and 2.3. The results from our two surveys are presented in Sect. 2.4. The discussion of the dust disc mass evolution as a function of the age of the systems, compared with the history of our solar system, is presented in Sect. 3. A detailed analysis of the debris disc properties by modelling their spectral energy distribution (SED) is provided in Sect. 4 and finally the summary is presented in Sect. 5.

2. Observations

2.1. Sample

Nearby sources ($d < 150$ pc) were selected from *The Formation and Evolution of Planetary Systems (FEPS) Spitzer* Legacy Program (Meyer et al. 2006). The FEPS sample contains 314 stars with stellar masses between ~0.5 and 2 $M_{\odot}$, ages spanning the range from 3 Myr to 3 Gyr and spectral types between K7 and F5. In addition, 14 objects were initially included in the FEPS sample because of an infrared excess previously detected with IRAS/ISO. Since these sources can introduce a bias in the FEPS sample with respect to the presence of a disc, they are not taken into account in any statistical analysis in this paper.

The characteristics of the entire star sample have been extensively analysed by the FEPS team (e.g. Meyer et al. 2006; Mamajek & Hillenbrand 2008). The stellar ages are based on pre-main sequence tracks for stars younger than 10 Myr, X-ray activity and the strength of the CaII H and K emission for nearby solar-type stars (≤50 pc), and the association of stars with clusters or star-forming regions of known age. A new calibration presented in Mamajek & Hillenbrand (2008) has been applied. Final ages will be presented by Hillenbrand et al. (in preparation; see also Mamajek & Hillenbrand 2008). The distances of the sources were determined by the FEPS team on the basis of Hipparcos parallaxes for nearby stars and kinematic distances for stars associated with young moving groups and associations. Our total sample contains 141 sources of which:

- 16 targets were observed at 350 μm with the CSO (*Caltech Submillimetre Observatory*) 10-m telescope (see Col. 6 Table 1);
- 40 targets were observed at 1.2 mm with the IRAM (*Institut de Radioastronomie Millimétrique*) 30-m telescope (see Col. 7 Table 1);
- 121 targets are taken from the SEST (*Swedish-ESO Submillimetre Telescope*) and OVRO (*Owens Valley Radio Observatory*) surveys performed by Carpenter at. al (2005), of which 17 have been re-observed during our surveys.

The sample includes 15 sources younger than 10 Myr, 16 intermediate-age systems (10–20 Myr) and 110 evolved systems (>20 Myr). In Sect. 3 we only consider the evolved systems in order to search for a correlation between the mass of the debris disc and the age of the system. In particular, 104 out of the 110 evolved systems are analysed excluding the sources not compatible with the FEPS sample selection (see above). The 104 sources analysed here include 45% of the FEPS sample older than 20 Myr and in particular: 35% of the systems with no infrared excess (until 70 μm) and 89% with excess.

2.2. CSO observations at 350 μm

Observations of the sources listed in Table 1 were carried out at the CSO between 17 and 21 April 2005, using the Submillimetre High Angular Resolution Camera II (SHARC-II) with the 350 μm filter. The full width at half maximum ($FWHM$) for the 10.4 m telescope beam profile is 8.5″ at this wavelength. The median zenith opacity at 225 GHz was 0.04. The typical on-source integration times varied from 40 min to 2 h depending on source elevation and zenith opacity, although a deeper 3.5 h integration was obtained for HD 107146 (see Corder et al. 2009). Pointing and instrumental flux calibrators were selected from the CSO SHARC-II list of calibrators. Data imaging and reduction were carried out using the Comprehensive Reduction Utility for SHARC-II. The errors associated with each detection are the quadratic sum of the instrumental error (between 5.3 and 45 mJy) and the calibration errors (between 12% and 22% of the flux). Instrumental errors are computed based on the rms computed in a sky annulus, and propagated over the photometric aperture. Calibration errors were determined based on repeatability of the flux calibrators over the entire observing run.

Table 1. The stellar properties, e.g. spectral type, temperature, luminosity and age range are reported in the first columns (from Meyer et al. 2006, 2008, Hillenbrand et al. 2008). CSO 350 μm and IRAM 1.2 mm measured fluxes and upper limits are reported in the sixth and seventh column. The detected sources are highlighted in bold. In the ninth column are the references to the stellar distances (listed in the eighth column).

Source	Spectral Type	$T_{\rm eff}$ [$^{\rm o}$K]	$\log(L_\star/L_\odot)$	log(Age)	$S^{\star}_{350\,\mu{\rm m}}$ [mJy]	$S^{\star\star}_{1.2\ {\rm mm}}$ [mJy]	Distance [pc]	Ref.
FEPS sources older than 10 Myr								
HD 60737	G0	5895	0.01	8.0–8.5		<4.5	38 ± 2	(2)
HII1101	G0V	5988	0.08	8.0–8.5		<2.3	133 ± 4	(5)
HII152	G5V	5823	−0.10	8.0–8.5		<2.7	133 ± 4	(5)
HII1200	F6V	6217	0.35	8.0–8.5		<2.3	133 ± 4	(5)
HD 90905	G1V	6028	0.16	8.0–8.5		<3	32 ± 1	(2)
HII514	—	5727	0.11	8.0–8.5		<2.6	133 ± 4	(5)
HD 104860	F8	5950	0.12	8.0–8.5	50.1 ± 9.3	4.4 ± 1.1	48 ± 2	(2)
HD 377	G2V	5852	0.09	8.0–8.5		4.0 ± 1.0	40 ± 2	(2)
HD 61005	G8V	5456	−0.25	8.0–8.5	95 ± 12		35 ± 1	(2)
HD 107146	G2V	5859	0.04	8.0–8.5	319 ± 6		29 ± 1	(2)
HD 72687	G5V	5738	−0.05	8.0–8.5	<54		46 ± 2	(2)
HII250	—	5767	−0.04	8.0–8.5		<3.28	133 ± 4	(5)
HD 219498	G5	5671	0.69	8.5–9.0		<4.8	150 ± 13	(3)
HD 61994	G6V	5538	0.01	8.5–9.0		<2.6	28 ± 2	(2)
HD 145229	G0	5893	−0.02	8.5–9.0	<22.5	<2.8	33 ± 1	(2)
HD 150706	G3(V)	5883	−0.02	8.5–9.0		<3.2	27 ± 1	(2)
HD 204277	F8V	6190	0.29	8.5–9.0		<2.1	34 ± 1	(2)
HD 85301	G5	5605	−0.15	8.5–9.0	<17.4	<2.7	32 ± 1	(2)
HD 69076	K0V	5405	−0.28	9.0–9.7	<42	<2.1	34 ± 1	(2)
HD 205905	G2V	5925	0.04	9.0–9.7		< 4.6	26 ± 1	(2)
HD 201219	G5	5604	−0.16	9.0–9.7		<4.1	36 ± 2	(2)
HD 206374	G6.5V	5580	−0.17	9.0–9.7		<3.9	27 ± 1	(2)
HD 38529	G8III/IV	5361	0.82	9.0–9.7		<3.2	42 ± 2	(2)
HD 136923	G9V	5343	−0.29	9.0–9.7		<3.2	20 ± 1	(2)
HD 6963	G7V	5517	−0.26	9.0–9.7		<4.2	27 ± 1	(2)
HD 122652	F8	6157	0.18	9.0–9.7	<19.5	3.2	37 ± 1	(2)
HD 187897	G5	5875	0.12	9.0–9.7		<2.4	33 ± 1	(2)
FEPS sources older than 10 Myr not included in the statistical analysis								
HD 134319	G5(V)	5660	−0.14	7.5–8.0	<25.2	<8.5	44 ± 1	(2)
HD 191089	F5V	6441	0.50	8.0–8.5	54 ± 15	<3.6	54 ± 3	(2)
HD 25457	F7V	6172	0.32	8.0–8.5		<2.2	19 ± 1	(2)
HD 8907	F8	6250	0.32	8.5–9.0		3.2 ± 0.9	34 ± 1	(2)
FEPS sources younger than 10 Myr								
[PZ99] J161411.0-230536	K0	4963	0.50	6.5–7.0	<21.9	3.5 ± 1.1	145 ± 2	(1)
RXJ1612.6-1859a	K0IV	5372	0.38	6.5–7.0	43 ± 8.7	5.9 ± 1.4	145 ± 2	(1)
HD 143006	G6/8	5884	0.39	6.5–7.0	1400 ± 39		145 ± 2	(1)
SCOPMS214	K0IV	5318	0.26	6.5–7.0	<72		145 ± 2	(1)
RX J1842.9-3532	K0IV	4995	−0.01	6.5–7.0	650 ± 29		130 ± 10	(3)
RX J1852.3-3700	K3	4759	−0.23	6.5–7.0	1200 ± 45		130 ± 10	(3)
HD 35850	F7/8V	6047	0.25	7.0–7.5		<3.7	27 ± 1	(2)
HE848	F9V	6309	0.47	7.5–8.0		<3.1	176 ± 5	(4)
HD 77407	G0(V)	5986	0.08	7.5–8.0		<3.45	30 ± 1	(2)
HD 22179	G0	5986	0.36	7.5–8.0		<3.3	100 ± 20	(3)
HD 12039	G3/5V	5688	−0.05	7.5–8.0		<2.7	42 ± 2	(2)
HD 70573	G1/2V	5896	0.14	7.5–8.0		<2.73	46 ± 15	(3)
HE750	F5	6421	0.28	7.5–8.0		<4.60	176 ± 5	(4)
HD 135363	G5(V)	4728	−0.48	7.5–8.0		<2.22	29 ± 1	(2)
Not in the FEPS list								
HD 82943						<27.9		
HD 38207	F2V	6769	0.72	8.0–8.5		<0.33	127 ± 25	(3)
HD 117176						<14.1		
HD 218738					<21.9	<3.3		

* The errors and the upper limits refer to the statistical errors (flux rms) and do not include the calibration uncertainty (between 12 and 22% of the flux). ** The errors and the upper limits refer to the statistical errors (flux rms) and do not include the calibration uncertainty (between 11 and 16% of the flux). Distance references: [1] de Zeeuw et al. (1999); [2] Perryman et al. (1997); [3] Hillenbrand et al.(2008); [4] Pinsonneault et al. (1998); [5] based on recent Pleiades distances: de Zeeuw et al. (1999), Zwahlen et al. (2004), Soderblom et al. (2004) and Pan et al. (2004).

2.3. IRAM observations at 1.2 mm

Millimetre continuum observations of 40 sources at 1.2 mm were carried out between May and December 2005 (*Projects num. 013-05, 141-05*) and between January and April 2008 (*Project num. 185-07*) at the IRAM 30-m telescope at Pico Veleta with MAMBO2, the 117 channel IRAM bolometer. The *FWHM* of the 30-m telescope beam is 11″ at 1.2 mm. The median zenith opacity at 230 GHz was 0.5 during the first run between May and November 2005, and 0.3 during the second run carried out in December 2005 and during the last run in 2008. Pointing and calibrator sources were selected from a standard list provided by IRAM. The observations were carried out in *on-off integration mode* using a standard calibration. An rms of 0.7 mJy was obtained in one hour (blocks of three times 20 min) of on-off integration. The weather conditions were stable during most of the nights and the calibrators were observed within a few hours from the science targets. The data were reduced with the data reduction package MOPSIC (Zylka 2006).

Observations of the same target at different dates were coadded to increase the signal to noise. The uncertainties associated with each flux are the quadratic sum of the statistical error and the calibration error. The statistical error is the rms of the flux over the entire telescope field of view, while the calibrator error is based on the agreement between the predicted calibrator fluxes and those measured over 48 h before and after the observations. We obtained statistical errors between 0.8 and 2.8 mJy and calibration errors between 11% and 16% in flux. The final uncertainties are dominated by the statistical error in the IRAM observations.

2.4. Detections and upper limits

The fluxes (in the case of detections) and the 3σ upper limits (in the case of non-detections) measured at 350 μm and 1.2 mm are listed in Table 1. The detection errors and the upper limits include only the statistical error. The calibration uncertainty is reported in the note to Table 1. The 3σ upper limits were computed as 3 times the statistical error described above. 31 sources have been observed with IRAM, 7 sources only with CSO and 9 sources with both telescopes. We detected 11 sources in total: 5 sources with IRAM, 8 with the CSO. Two of the sources were detected with both IRAM and CSO. Five of them are primordial discs younger than 10 Myr, and six are debris discs. All sources were unresolved with the exception of HD 107146 which had a deconvolved size at 350 μm of $8\farcs9 \times 8\farcs2$ with an uncertainty of about $0\farcs6$ per axis (Corder et al. 2009).

3. Disc dust mass

The main goal of this project is to analyse the temporal evolution of circumstellar debris discs and the mechanism of their dissipation around solar-type stars.

The dust mass in debris discs is expected to decrease with time. Depending on which process (collisions or Poynting-Robertson drag) is the main driver of dust removal, we expect a different power-law dependence of the dust mass as a function of the age of the system (Dominik & Decin 2003).

In this analysis we include the dust masses computed from the *millimetre* observations of nearby solar-type stars obtained with IRAM presented here and with SEST and OVRO (from C05).

The disc is assumed to be isothermal and optically thin ($\tau \ll 1$) at millimetre wavelengths. The dust disc mass can then be derived from the millimetre flux, using the following equation:

$$M_{\rm dust} = \frac{S_\nu D^2}{k_\nu B_\nu(T_{\rm dust})} \quad (1)$$

where $k_\nu = k_0(\nu/\nu_0)^\beta$ is the mass absorption coefficient, β parametrises the frequency dependence of k_ν and S_ν is the observed flux. D is the distance to the source, $T_{\rm dust}$ is the dust temperature and $B_\nu(T_{\rm dust})$ is the Planck function.

In order to be consistent with C05, we compute the dust masses assuming $\beta = 1$, $k_0 = 2$ cm^2 g^{-1} at 1.3 mm (Beckwith et al. 1990) and $T_{\rm dust} = 40$ K.

The uncertainty in the dust mass is computed using error propagation. In the following, we discuss the principal systematic errors which are present in the final dust mass uncertainty. The mass absorption coefficient is poorly constrained. We consider as limit the commonly used value for debris discs of $k_0 = 1.7$ cm^2 g^{-1} at 800 μm adopted by Zuckerman & Becklin (1993), which corresponds to $k_0 = 1.0$ cm^2 g^{-1} at 1.3 mm. The mass absorption coefficient alone introduces at least a factor 2 in the final uncertainty associated to the mass. In order to be consistent with the previous analysis of C05, we adopted a temperature of 40 K. This represents a compromise between the temperature associated with cold dust in protoplanetary discs ($T \sim 20$–30 K, e.g. Beckwith et al. 1990) and warm dust in debris discs ($T \sim 40$–100 K; Zuckerman & Song 2004a).

Since the mass is proportional to $T_{\rm dust}^{-1}$, the temperature alone introduces a factor of 2 in the uncertainty of the masses.

Another source of uncertainty in the final mass error is introduced by the source's distance. Nevertheless, the parallax of most of the sources older than 20 Myr (which will be in the following analysed), has been measured by *Hipparcos*, and the distance uncertainty is directly computed from the parallax uncertainty. This contributes an uncertainty of at least ∼10% of the dust masses.

The 3σ upper limits to the dust mass have been computed when the sources were not detected with a signal to noise ratio of at least three.

The mass of the newly observed sources younger than 20 Myr is also plotted as reference[1]. Taking into account the uncertainty on distance, temperature, measured flux and mass absorption coefficient, the final uncertainty is ∼55% of the dust mass.

3.1. Evolution of the dust mass

Mass detections and upper limits are presented in Fig. 1 as a function of age. In total, we plotted 132 upper limits and 9 detections computed from the millimetre measurements. 17 sources have been observed in both surveys, C05 and with IRAM (connected by a dotted line in Fig. 1). Due to the higher sensitivity of the IRAM bolometer compared to SEST and OVRO, we detected 4 discs with dust masses down to 5×10^{-7} $M_\odot$, about one order of magnitude smaller than those in C05.

Primordial discs are shown in Fig. 1 only as comparison with systems older than 20 Myr but they are not taken into account in any statistical analysis in this paper.

The other variable which can strongly affect our analysis is the age determination of the discs older than 20 Myr. Their ages derived using different techniques are summarised in Table 2.

[1] Note however, that the assumption of optically thin emission at millimetre wavelength cannot be generalised to all primordial discs

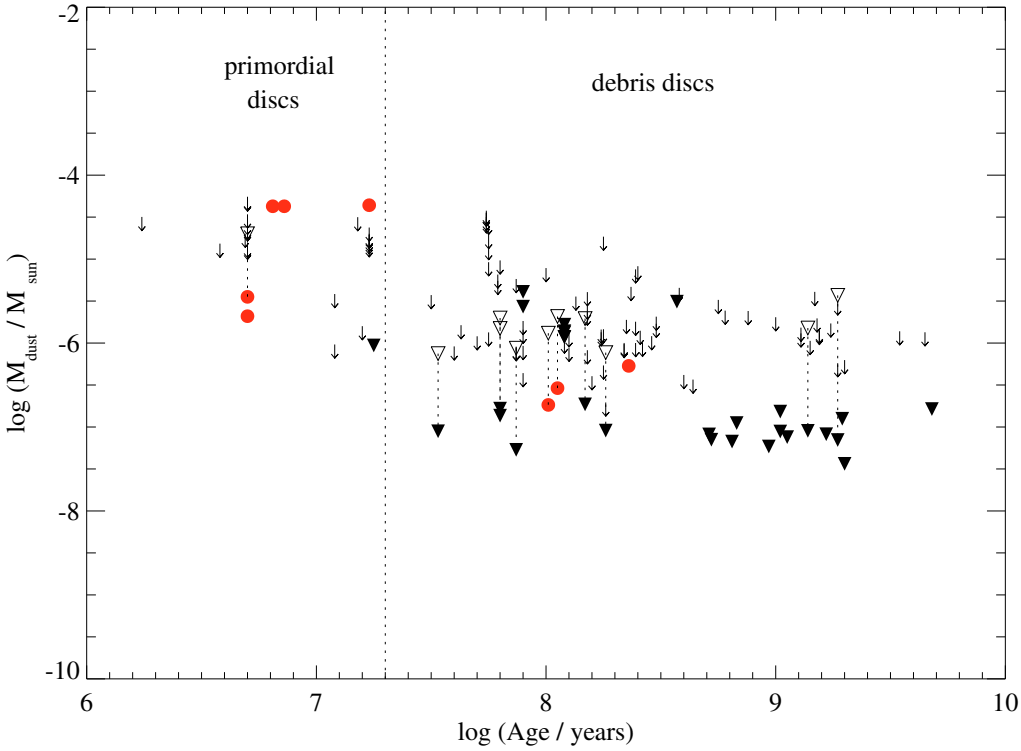

Fig. 1. Disc mass versus age of the system. Filled circles are the masses determined from the IRAM detections (this work) and from the detections presented by C05. Upper limits are shown as filled triangles (new IRAM observations), empty and filled triangles (objects measured by C05 and re-observed here with higher sensitivity) and down arrows (from C05). The sources observed in both studies are connected by dashed lines. The vertical line separates the sources younger than 20 Myr and evolved systems older than 20 Myr.

Table 2. Ages (in logarithmic scale) of the debris discs detected at the millimetre wavelength, with IRAM (this work), SEST and OVRO (from C05). They have been derived using different techniques: the strength of the CaII H and K (R'_{HK}) and Lithium (Li) emission, X-ray activity (*X-ray*), and the rotational period-age (p_{rot}) relation (L. Hillenbrand, private communication). The ages are averaged and the standard deviation is adopted as error.

Method	HD 377	HD 8907	HD 104860	HD 107146
R'_{HK}	8.34	8.78	8.44	8.09
$v \sin i$	7.99	8.1	–	8.89
p_{rot}	–	–	7.62	–
X-ray	7.9	7.88	8.06	–
Li	7.8	9.28	8.08	8.1
average	8.01	8.51	8.05	8.36
stdev	0.23	0.64	0.34	0.46

The final ages are computed as the average and the standard deviation is adopted as uncertainty (Table 2). A more detailed discussion of the ages of the whole FEPS sample will be presented by Hillenbrand et al. (in preparation; see also Mamajek & Hillenbrand 2008).

In the following subsection we present the statistical analysis aimed at constraining the physical characteristics of the dust in circumstellar discs at ages older than 20 Myr, in order to understand the timescale and the dissipation mechanism in debris discs.

3.1.1. Method: statistical analysis

A quantitative analysis of the dust mass-age relation was performed for systems older than ~20 Myr. We carried out a *survival analysis* (Feigelson & Nelson 1985) in order to include the information contained in the dust mass upper limits derived from the millimetre non-detections. We use the program ASURV Rev. 1.2 (Lavalley et al. 1992), which implements the survival analysis methods presented in Feigelson & Nelson (1985) and Isobe et al. (1986).

The *generalised Kendall's tau correlation* (Brown et al. 1974) was used to measure the degree of correlation between age and disc mass among debris discs. Such a method includes the analysis of both detections and upper limits. The probability that the disc mass is correlated with the age is 76%.

To determine whether there is a different dust mass distribution in debris disc systems older than 20 Myr, we used *two-sample tests*. We applied three different tests: the Gehan, logrank, and Peto-Prentice tests (e.g. Feigelson & Nelson 1985). In order to investigate the evolution of the debris dust we divided the sample of objects older than 20 Myr in two sub-samples with almost the same number of objects: the first with ages between 20 and ~180 Myr, and the second sub-sample with ages between ~180 Myr and 5 Gyr.

The three *two-sample tests* give a probability between 70 and 83% that younger and older debris systems belong to different parent populations in terms of dust mass. The relatively low significance of our results comes from the low number of detected sources, compared to the upper limits, and the narrow range in age of the detected debris discs. This leads to a high probability to assign a detected disc to a different sub-sample in age. We could not perform any conclusive linear regression to the data points since the detected objects span a very narrow range in age and masses, and in general there are too many upper limits compared to detections.

3.2. Discussion

The detection limit of our survey does not allow us to draw any firm conclusion about the evolution of the debris dust around solar-like stars as a function of age. Even more sensitive millimetre observations are needed to find statistically reliable trends. Our sample is biased toward sources with infrared excess. However, with the current sensitivity limit, additional observations of sources without infrared excess, which have a lower probability to be detected in the millimetre, would only increase the number of upper limits. This would not change the result of our statistical analysis.

We recall that all the mass derivations are valid only if the mass absorption coefficient k, which is inversely proportional to the mass of the dust in the disc, remains constant with time.

While in the protoplanetary disc phase we would expect a strong change of the mass absorption coefficient with time, in the debris disc phase we expect an equilibrium phase which is characterised by an almost constant second generation of dust. The assumption of a roughly time-independent dust opacity seems to be reasonable as long as we consider discs in the debris phase.

4. SED analysis of debris discs detected at 350 μm and/or 1.2 mm

The debris discs detected by our surveys offer the opportunity to characterise and compare the disc properties around solar type stars. This is the case for the following objects: HD 104860, HD 8907, HD 377, HD 107146, HD 61005 and HD 191089.

We compiled the spectral energy distributions from the infrared data available in the literature and our new detections at sub-millimetre and/or millimetre wavelengths. Synthetic photometric points at 13 and 33 μm, derived from the IRS spectrum (Hillenbrand et al. 2008), were also included in the SEDs. These data points allow us to distinguish the infrared excess of the debris disc from the stellar photosphere, determined by a Kurucz model. The IRS spectrum is overplotted in Figs. 2–7, but was not considered during the SED modelling.

To further characterise the debris discs detected during our survey, we compute:

- the β index from their SED to derive the dust grain size present in the disc;
- the collisional and Poynting-Robertson drag timescales;
- the blowout grain size ($a_{\rm blow}$);
- best fit model parameters by modelling the SED.

β index – In the millimetre wavelength range, where $h\nu/KT \ll 1$, the Planck function can be approximated with the Rayleigh-Jeans relation ($B_\nu \sim 2k\nu^2Tc^{-2}$). The disc is assumed to be optically thin with the optical depth $\tau_\nu(r) = k_\nu \sum(r) < 1$. Under these conditions $F_\nu \sim k_\nu \nu^2 \frac{4\pi k}{D^2} \int_{R_{\rm in}}^{R_{\rm out}} \Sigma(r)T(r)r{\rm d}r$. At wavelengths $\lambda > 0.1$ mm the mass absorption coefficient k_ν is $k_\nu \propto \nu^\beta$, where β is the dust opacity index. Since the slope of the SED in the millimetre wavelength range is proportional to ν^α, the measure of the spectral index α enables us to directly constrain the β index via the relation $\beta = \alpha - 2$ and to derive the index β. The index β is 2 for interstellar medium grain sizes, between 0 and 2 for pebbles of the order of 1 mm in size, and 0 for even larger grains (e.g. Beckwith et al. 2000). The slope α of the SED in the sub-millimetre/millimetre wavelength range is derived, using a linear regression that gives the errors in slope of the best-fit. The values for the β index of the power law of the dust absorption coefficient are always <1 (see Table 3), which suggests the presence of dust with at least millimetre size particles (e.g. Henning & Stognienko 1996; Rodmann et al. 2006).

Blowout grain size – Small grains are affected by the interaction with the stellar radiation field. This causes a force acting on the particles which is parametrised by the ratio of the radiation force to the stellar gravity. We compute the blowout grain size ($a_{\rm blow}$) in the debris disc systems using the equations presented in Hillenbrand et al. (2008; based on Burns et al. 1979; and Backman & Paresce 1993):

$$a_{\rm blow} = 0.52\,\mu{\rm m}\frac{2.7\ {\rm g/cm^3}}{\rho}\frac{1+p}{1.1}\frac{L_\star/L_\odot}{(M_\star/M_\odot)(T_\star/5780)} \quad (2)$$

where, ρ is the grain density, p the grain albedo (0.1 for silicate grains) and a the grain radius. Sub-micron sized particles are therefore blown out from the disc near a Sun-like star.

Poynting-Robertson and collisional timescales – Defining $\eta_0 = t_{\rm PR}/t_{\rm coll}$ (Wyatt et al. 1999–2005), where $t_{\rm PR}$ and $t_{\rm coll}$ are the Poynting-Robertson drag ($t_{\rm PR}$) and collisional timescales respectively, it is possible to distinguish between discs in collisional regime ($\eta_0 \gg 1$) and Poynting-Robertson drag regime ($\eta_0 \ll 1$). When $\eta_0 \gg 1$ the disc is dense and the collisions occur faster than the P-R drag: the dynamically bound dust remains at the same radial location as the planetesimals, while unbound grains are blown out and their surface density distribution falls off as r^{-1} (where r is the distance from the star).

The Poynting-Robertson drag ($t_{\rm PR}$) and collisional timescales ($t_{\rm coll}$) of the debris discs are computed, using the equations presented in Hillenbrand et al. (2008; based on Burns et al. 1979; and Backman & Paresce 1993):

$$t_{\rm PR} = 720\ {\rm yr}\frac{(\rho/g/{\rm cm^3})(a/\mu{\rm m})(r/{\rm AU})^2}{(L_\star/L_\odot)(1+p)} \quad (3)$$

where, ρ is the grain density, p the grain albedo (again 0.1 for silicate grains) and a the grain radius. We assume silicate grains of 10 μm in size and a grain density of 2.7 g/cm^3 at the inner radius of the disc (computed by our model, see Table 4).

Under the assumption of circular orbits and completely destructive collisions between grains of the same size, the collisional timescale is computed using the equation:

$$t_{\rm coll} = \left(\frac{r}{\rm AU}\right)^{1.5}\frac{1}{9\sigma(r)\sqrt{M_\star/M_\odot}}\ {\rm yr} \quad (4)$$

where $\sigma(r)$ is the face-on fractional surface density: for a constant surface density, $\sigma(r) = 2f/\ln(R_{\rm OUT}/R_{\rm in})$, with $R_{\rm in}$ the inner disc boundary, $R_{\rm OUT}$ the outer disc radius and $f = L_{\rm dust}/L_\odot$ (e.g., Backman 2004).

The collisional timescale has been computed for grains of 10 μm in size at the inner radius of the disc (computed by our model, see Table 4). According to Wyatt (2005), the ratio $t_{\rm coll}/t_{\rm PR}$ is proportional to $1/\sqrt{a}$, where a is the grain size.

These values are summarised in Table 3.

SED modelling – The SEDs were modelled using the radiative transfer model of Wolf & Hillenbrand (2003).

The model assumes that the dust grains are compact spherical particles heated only by the direct stellar radiation. The interaction between stellar radiation and dust particles can be described by the following radiative processes: scattering (neglecting multiple scattering), absorption and re-emission of stellar radiation by dust grains. The disc is then checked to be optically thin to the stellar radiation and to the dust re-emission at all wavelengths. The contribution to the SED from a single

Table 3. Blowout grain size, P-R drag timescales of the debris discs detected in the CSO and/or IRAM surveys. The β-index discs only for the stars with the SED sampled in the submillimetre/millimetre range (details in Sect. 4) is reported.

HD 104860	HD 8907	HD 377	HD 107146	HD 61005	HD 191089	
$a_{\rm blow,Si}$ [μm]	0.64	0.81	0.54	0.49	0.34	1.14
$t_{\rm P-R,Si}$ [Myr]	0.39	0.5	0.03	0.08	9.85	1.86
$t_{\rm coll}$ [Myr]	0.007	0.007	0.003	0.002	0.009	0.005
β	0.5 ± 0.7	–0.1 ± 1.3	–	0.4 ± 0.2	–	–

Table 4. Model results, reduced χ^2 ($\chi^2_{\rm red.}$) assuming a fixed outer radius ($R_{\rm OUT}$) of 150 AU and a maximum grain size ($a_{\rm max}$) of 3 mm.

	HD 104860	HD 8907	HD 377	HD 107146	HD 61005	HD 191089
$M_{\rm dust}/M_{\oplus}$	0.082 ± 0.007	0.040 ± 0.005	0.058 ± 0.013	0.110 ± 0.008	0.261 ± 0.023	0.110 ± 0.037
$R_{\rm in}$ [AU]	21 ± 5	27.8 ± 13.9	6.1 ± 0.8	10.2 ± 0.8	95.6 ± 23	79 ± 98
$a_{\rm min}$ [μm]	8 ± 2	6 ± 2	14 ± 5	8.6 ± 1.2	0.4 ± 0.3	0.23 ± 0.78
$\chi^2_{\rm red.}$	2.6	4.3	5.0	4.5	16.3	8.7

dust grain results from the integration of the scattering and re-emission processes over all wavelengths. Finally the emergent spectrum is the sum of all the dust grain contributions.

The model parameters are the radiation emitted by the central star, the total disc mass, the disc size, the radial density distribution, the minimum and maximum grain size in the disc, the grain size distribution, and the chemical composition of the grains. The radial density distribution is described by a power-law, $n(r) \propto r^{-q}$ where $q = 1$ corresponds to a disc with a constant surface density $\Sigma(r) \propto r^0$. The grain size distribution is also described by a power-law $n(a) \propto a^{-p}$ where the canonical value $p = 3.5$ characterises a size distribution initially produced by a collisional cascade. We always use this grain size distribution in our models. For each grain size a temperature distribution over the disc size is computed.

The model parameter space has been extensively analysed by Wolf & Hillenbrand (2003). They found that the increase of the inner radius $R_{\rm in}$ causes a loss of the warm dust that is mainly responsible for the near-infrared (NIR)/ mid-infrared (MIR) shape of the SED; the excess emission over the stellar photosphere starts at longer wavelengths. This is more pronounced when the minimum grain size $a_{\rm min}$ increases, because the main contribution to the NIR/MIR spectrum at high temperatures comes from small grains. The presence of an inner gap causes the loss of warm dust which is mainly responsible for the NIR/MIR shape of the SED. Increasing the size of the gap, the MIR flux decreases and the excess is shifted to longer wavelengths. Keeping the disc mass constant, the flux in the millimetre region increases slightly, but the net flux is smaller compared to a disc without an inner gap. This is because the fraction of the stellar flux absorbed by a single dust grain decreases with increasing radial distance from the star.

We assumed *astronomical silicate* grains (optical data from Draine & Lee 1984; and Weingartner & Draine 2001) since they are expected to be the main component of the dust in protoplanetary discs (Pollack et al. 1994).

Since the outer radius cannot be constrained from the SED alone, it was assumed to be 150 AU, consistent with the location of the most distant object of the Kuiper belt in our Solar System (e.g. Gladman et al. 2002). The choice of such a value is supported by a recent resolved millimetre map of one of the debris discs analysed (Corder et al. 2009), where the millimetre emission is extended up to 150 AU from the central star. The maximum grains size is assumed to be 3 mm, since the β index measurements suggested the presence of at least millimetre-sized particles in the discs; this is the grain size which strongly contributes to the millimetre emission that we detect. The Levenberg-Marquardt method was applied to find the best-fit parameters of the model leaving the *inner radius* ($R_{\rm in}$), *minimum grain size* ($a_{\rm min}$) *and dust mass* ($M_{\rm dust}$) as free parameters.

The reduced χ^2, associated with each best-fit model, was computed for each fit normalising the standard statistic χ^2 to the number of free parameters of the fit (Bevington 1969). These parameter uncertainties are estimated from the covariance matrix (inverse of the χ^2 curvature function) by the Levenberg-Marquardt algorithm. The modelling results are listed in Table 4. The degeneracy of the SED models was checked using the σ-confidence regions delineated by lines of constant $\Delta\chi^2$. The model parameter space ($R_{\rm in} \times M_{\rm dust} \times a_{\rm min}$) was explored around the best fit values. The 2-dimensional confidence regions in Figs. 2–7 are the projections of the 3-dimensional isosurfaces defined by fixed $\Delta\chi^2$ (e.g. Press et al. 1992). The shape of the confidence regions confirm an intrinsic degeneracy of our model probably between inner radius, minimum grain size and dust mass.

4.1. HD 104860

HD 104860 is an F8 star at a distance of 47 pc from the Sun. It was classified as a γ Doradus variable candidate by Handler (1999). Wichmann et al. (2003) identified the object as a young zero age main sequence star using LiI in absorption (Wichmann et al. 2003). In Table 2 we summarise the ages derived from different methods (L. Hillenbrand, private communication). The average age is ~140 Myr, the value that we adopted in our analysis.

The SED of HD 104860 is presented in Fig. 2. It includes the Spitzer/IRAC and Spitzer/MIPS photometry from 3.6 to 160 μm, synthetic photometry at 13 and 33 μm obtained from the IRS low resolution spectrum (Hillenbrand et al. (2008), our CSO and IRAM detections at 350 μm and 1.2 mm, SCUBA detections at 450 and 850 μm (Najita & Williams 2005), and an OVRO 3.1 mm upper limit (Carpenter et al. 2005). The infrared-excess emission detected by Spitzer suggests the presence of debris material around this main sequence star (Carpenter et al. 2008).

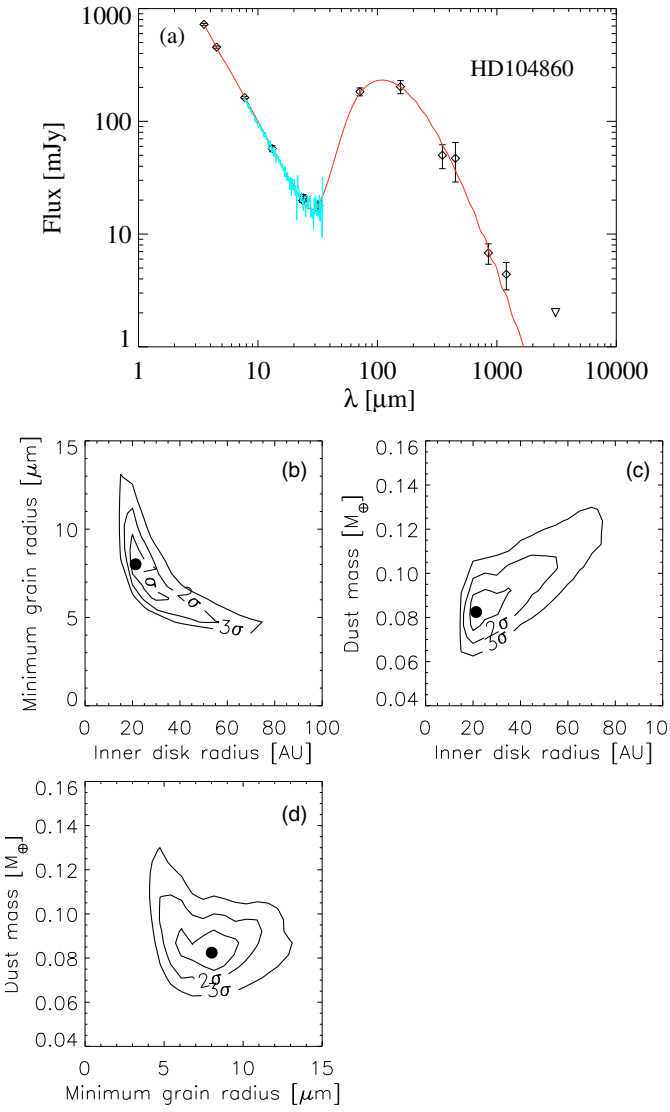

Fig. 2. SED of HD 104860 (upper plot **a**)) detections are shown as empty diamonds while 3σ upper limits are shown with empty triangles. The solid line shows the best fit model (see details in Sect. 4). The lower plots **(b–d)** represent the 2D projections of the 3D surfaces of constant $\Delta\chi^2$ obtained varying at the same time the dust mass, minimum grain size and inner disc radius.

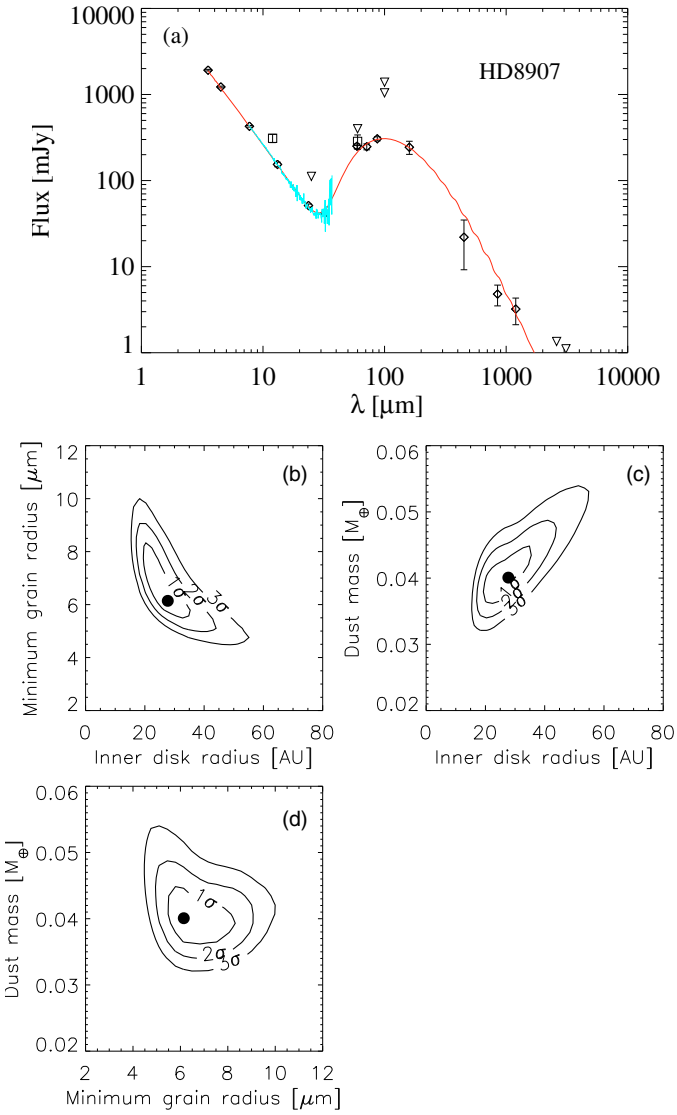

Fig. 3. As Fig. 2 but for HD 8907.

Early modelling of the spectral energy distribution of HD 104860 was presented by Najita & Williams (2005). Treating dust grains as simple blackbody radiators, their sub-millimetre observations at 450 and 850 μm indicate a dust temperature of $T_{\rm dust}$ = 33 K and a mass of the disc of 0.16 $M_\oplus$. Our new detection allows us to sample the SED at longer wavelengths and hence constrain the slope of the far-infrared to millimetre excess. The best-fit model parameters are reported in Table 4 and the computed best-fit model is plotted in Fig. 2. The confidence regions of the fit (see lower plots in Fig. 2) show some degree of degeneracy of the model. The dust mass is constrained between 0.07 $M_\oplus$ and 0.15 $M_\oplus$, while the inner radius is located between 10 and 50 AU and the minimum grain size is between 5 and 15 μm. The dust mass computed by the model (see Table 4) is of the same order of magnitude as the masses computed using a simple black-body model (Najita & Williams 2005) and Eq. (1). The minimum grain size obtained is one order of magnitude higher than the blowout grain size of the system. The confidence regions delineated by constant $\Delta\chi^2$ contours suggest that a minimum grain size of the same order of magnitude of the blowout size is a poor fit to the data.

4.2. HD 8907

HD 8907 is a F8 star, located at 34 pc from the Sun, which has already reached the main sequence. In our analysis we adopt an age of the system of 680 Myr, which is the average of the ages derived from different methods (Table 2, Hillenbrand, private communication).

The SED of HD 8907 is presented in Fig. 3. The ISO photometry at 60 and 90 μm are from Silverstone (2000), the SCUBA detections at 450 and 850 μm from Najita & Williams (2005), IRAM detection at 1.2 mm from this work and the OVRO 2.6 and 3.1 mm upper limits from C05. The IRAS detections (Helou & Walker 1988; empty squares in Fig. 3), are systematically larger than the Spitzer photometry, due to the bigger beam and they were not taken into account during the model fitting. The infrared excess detected by ISO (Zuckerman & Song 2004a) suggested the presence of debris dust. Under the assumption that the dust particles radiate as a black body, a temperature of ~60 K was inferred for particles orbiting at ~30 AU from the

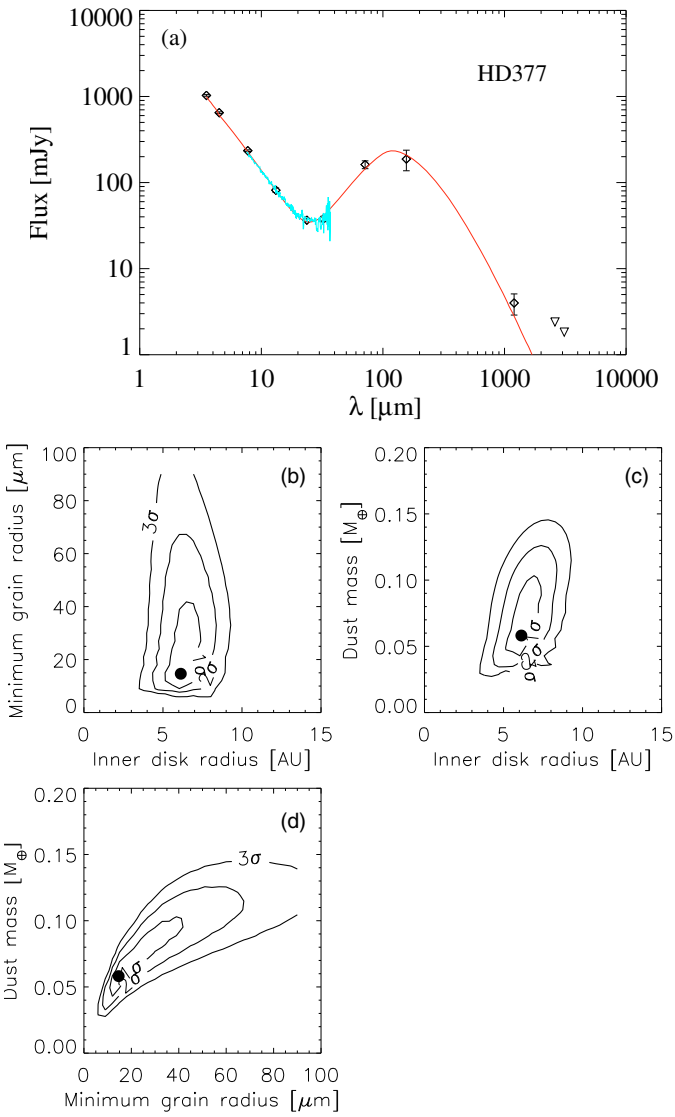

Fig. 4. As Fig. 2 but for HD 377.

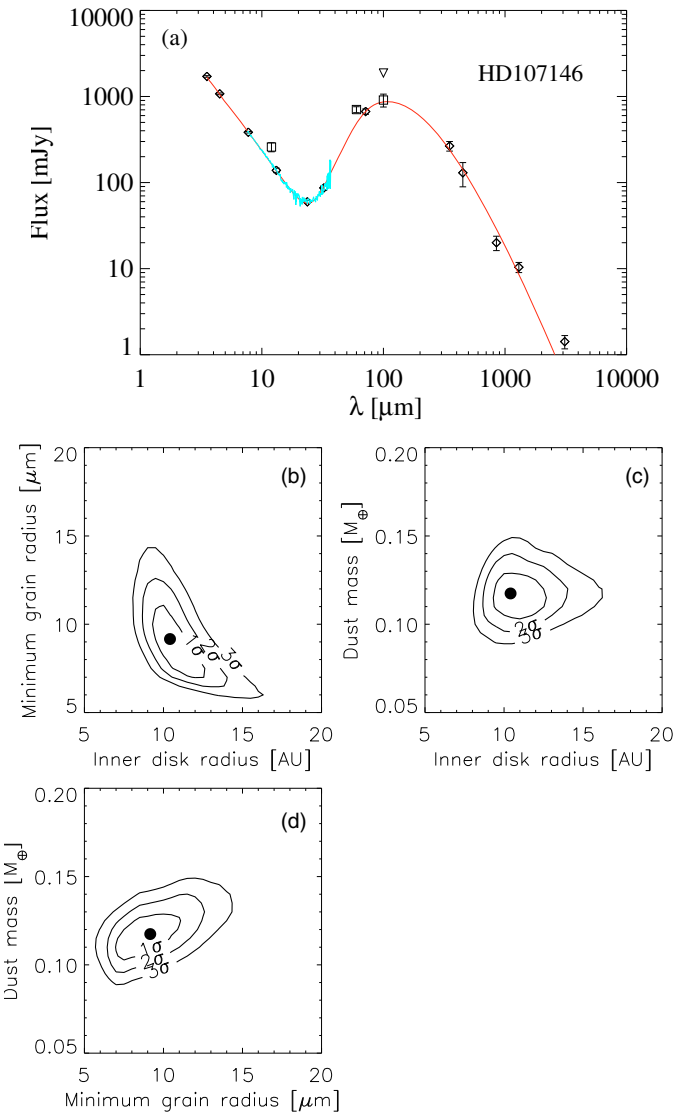

Fig. 5. As Fig. 2 but for HD 107146.

central star (Zuckerman & Song 2004a). The SED infrared excess has also been detected by Spitzer between 3.6 and 70 μm by Kim et al. (2005), and they found an inner radius of ~48 AU with a temperature of ~48 K.

Our new detection allows us to sample the SED at longer wavelengths and hence constrain the slope of the far-infrared to millimetre excess. The best-fit model parameters are reported in Table 4 and the computed best-fit model is plotted in Fig. 3. The confidence regions of the fit which show some degree of degeneracy of the model (see lower plots in Fig. 3): the dust mass is constrained between 0.03 $M_\oplus$ and 0.1 $M_\oplus$, while the inner radius is located between 15 and 30 AU and the minimum grain size is between 5 and 10 μm.

As in the case of HD 104860, the dust mass computed by the model of HD 8907 (see Table 4) is comparable to the value computed using Eq. (1). The minimum grain size is between 4 and 8 μm. This is one order of magnitude higher than the blowout grain size of the system and is consistent with previous modelling (Kim et al. 2005). The inner radius computed by our model is poorly constrained since it has an uncertainty of 50%.

4.3. HD 377

HD 377 is a G2V star at a distance of 40 pc which has already reached the main sequence. It is surrounded by a debris disc with a high fractional luminosity ($L_{\rm IR}/L_{\rm star}$), 4.0×10^{-4} (Moór et al. 2006). The ages of HD 377 derived from different methods (L. Hillenbrand, private communication) are summarised in Table 2. The average age is ~110 Myr, the value that we adopted in our analysis.

Pascucci et al. (2006) investigated the presence of gas in the disc of HD 377, but they did not detect any gas emission lines in the infrared nor in the millimetre wavelength range.

The SED was compiled from the literature including our new detection at 1.2 mm (Fig. 4). The OVRO 2.6 and 3.1 mm upper limits are from C05. The best-fit model parameters are reported in Table 4 and the computed best-fit model is plotted in Fig. 4. The confidence regions of the fit (see lower plots in Fig. 4) show a high degree of degeneracy of the model compared to the other debris discs modelled. This results from the poor constraints on the SED in the sub-millimetre region.

As for HD 104860 and HD 8907, the dust mass computed by the model (see Table 4) is comparable to the value computed using Eq. (1). The inner radius is the smallest in our sample, but the

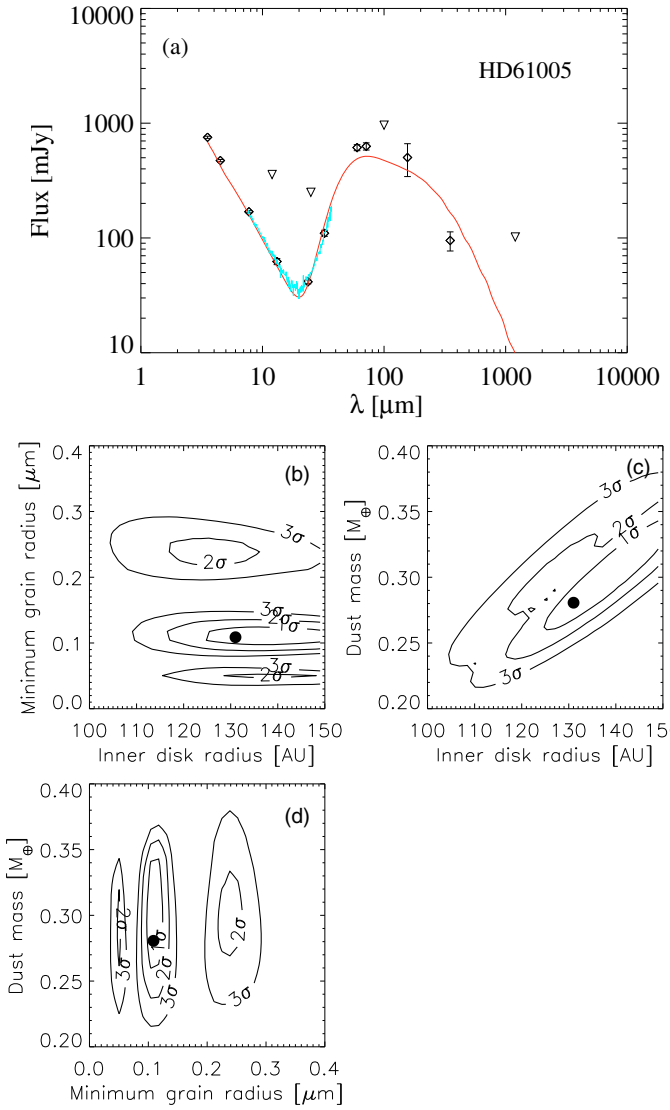

Fig. 6. As Fig. 2 but for HD 61005.

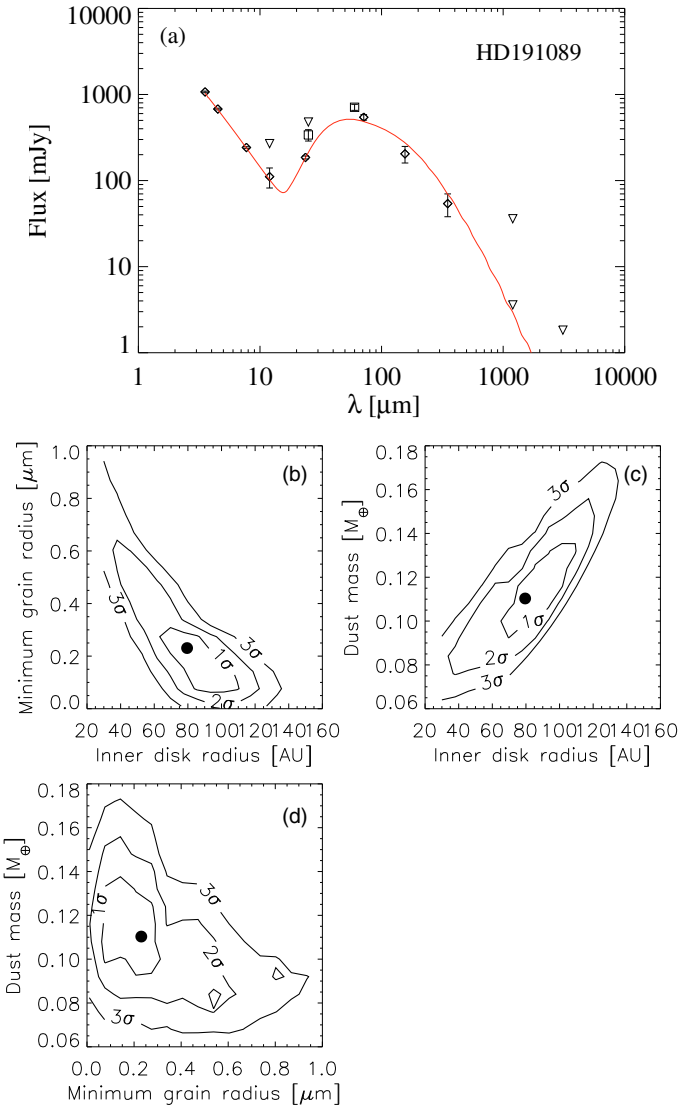

Fig. 7. As Fig. 2 but for HD191089.

disc seems to lack small dust grains with sizes up to 14 μm. The minimum grain size obtained is one order of magnitude higher than the blowout grain size of the system.

4.4. HD 107146

HD 107146 is a G2 V star located 28.5 pc from the Sun. The star is a candidate periodic V-band photometric variable (Koen & Eyer 2002). From the average between the ages derived with different methods (Table 2), we obtain an age of ~230 Myr. HD 107146 is also the first debris disc around a solar-type star resolved in scattered light by the Hubble Space Telescope (Ardila et al. 2004). They resolved a ring-like disc with most of the material concentrated between 86 and 130 AU, using a coronograph of 1.8″ in radius. The disc was also marginally resolved at 450 and 850 μm and the observations suggested the presence of an inner hole with a radius larger than 31 AU (Williams et al. 2004). Such an inner hole would also explain the lack of an IRAS 25 μm excess and a far-infrared excess at 60 and 100 μm (Silverstone 2000). C05 presented OVRO 3 mm images of this source. HD 107146 has also been resolved during our survey at 350 μm with CSO and at 1.3 mm with CARMA (Corder et al. 2009). The millimetre image shows a clumpy disc extended between ~60 AU and ~150 AU with a symmetric peak of the emission at ~97 AU from the central star.

The SED was compiled from the literature, including our new detection at 350 μm (Fig. 5) and the CARMA detection at 1.3 mm (Corder et al. 2009). HD 107146 is the only disc detected at 3.1 mm. The IRAS detections (Helou & Walker 1988; empty squares in Fig. 5), are systematically higher than the Spitzer photometry, due to the bigger beam and they were not taken into account during the model fitting. The best-fit model parameters are reported in Table 4 and the computed best-fit model is plotted in Fig. 5. The degree of degeneracy of the model is shown in the confidence regions of the fit (see lower plots in Fig. 5). The dust mass is constrained between 0.08 $M_{\oplus}$ and 0.15 $M_{\oplus}$, while the inner radius is located between 7 and 15 AU and the minimum grain size is between 8 and 15 μm. It is interesting to notice that the inner radius computed by our model, is more than 7 times smaller than the inner radius of the ring-like disc in the HST images. This is because different grain populations are traced by our model and the HST image: while the HST traces only the distribution of the sub-micron size population (below $a_{\rm blow}$), our model includes the re-emission from grains from micron to millimetre in size. This explanation is also supported by the resolved images in the sub-millimetre wavelength range of

HD 107146 which suggest the presence of grains at radii smaller compared to the ring-like structure seen in the HST image.

4.5. HD 61005

HD 61005 is a G3/G5V star with a Hipparcos distance of 35 ± 1 pc, located in the local bubble, a region that is thought to be almost completely free of diffuse dust clouds (Franco et al. 1990). From an average of the chromospheric activity available from the literature, and a new calibration of the chromospheric activity-age relation (FEPS, private communication), we adopt an age of 135 Myr. The SED was previously modelled by Hines et al. (2007): under the assumption that dust particles of ∼10 μm radiate as a black body with a temperature of ∼50–70 K, they obtained a minimum distance for the circumstellar material of ∼7 AU. This star was also monitored during a radial velocity survey looking for planets around active stars, but no planets were detected (Setiawan et al. 2008). HST/NICMOS observations (Hines et al. 2007) reveal dust-scattered starlight extending to distances of ∼240 AU from the occulted star. The structure is strongly asymmetric about its major axis, but is mirror-symmetric about its minor axis; morphologically, the object resembles a wing-spread moth with the star as the head.

HST scattered light images reveal a swept shape of the disc with an inner radius ≤10 AU and an outer radius up to 240 AU (Hines et al. 2007). Such emission is thought to be associated to the local interstellar medium that scatters the stellar light, so that the movement of HD 61005 through the medium causes the swept shape of the disc (Hines et al. 2007). These observations give a complementary picture of the circumstellar material present in the disc since different grain populations are traced in our model and in the scattered light images.

The SED was compiled from the literature including our new detection at 350 μm (Fig. 6) and the SEST upper limit at 1.2 mm from C05. The best-fit model parameters are reported in Table 4 and the computed best-fit model is plotted in Fig. 6. The confidence regions of the fit (see lower plots in Fig. 6) show that the best fit parameters represent only a local minimum of the model parameters space. This is probably due to the fact that the model assumptions are not valid in this case. As suggested from the HST images, the object seems to be located in the local interstellar medium material, which probably introduces an additional small grain population which contributes to the scattered light in the SED. Our model assumes that all the detected flux is stellar light scattered and/or absorbed and re-emitted only by the dust particles in the disc.

4.6. HD 191089

HD 191089 is an F5V star with a Hipparcos distance of 54 ± 3 pc from the Sun. This star was selected for the FEPS programme because it was known to have a debris disc based on ISO and IRAS measurements and it was not considered in our statistical analysis presented in Sect. 3. An upper limit of the age (∼3 Gyr) for the system was presented by Nordström et al. (2004), using main-sequence isochrones. We adopt an age of ∼300 Myr (Hillenbrand et al. 2008).

The SED was compiled from the literature (Fig. 7) including the Spitzer spectro-photometry (Carpenter et al. 2008), CSO detection at 350 μm and IRAM upper limit at 1.2 mm from this work and OVRO 3.1 mm upper limit from C05. The IRAS detections (Helou & Walker 1988; empty squares in Fig. 7), are systematically higher than the Spitzer photometry, due to the bigger beam and they were not taken into account during the model fitting. Since there is no IRS spectrum of the source constraining the beginning of the infrared excess close to the stellar photosphere, the IRAS detection at 12 μm was taken into account during the SED fitting. The best-fit model parameters are reported in Table 4 and the computed best-fit model is plotted in Fig. 7. The confidence regions of the fit show some degree of degeneracy of the model (see lower plots in Fig. 7). We note that the model result is not significant at all. This is due to the few data points which constrain the SED.

4.7. Modelling discussion

Comparing the collisional timescale to the Poynting-Robertson timescale, we conclude that all the detected debris disc are systems in the collision dominated regime.

The SED of the debris discs has been modelled leaving 3 parameters simultaneously free: inner radius, dust mass and minimum grain size.

We notice that the slope of the SEDs seems to change from the sub-millimetre to the millimetre wavelength range, but is well reproduced by our models within the errors. Including grains larger than 3 mm in the model would decrease the steepness of the slope in the sub-millimetre, but would not reproduce at the same time the sub-millimetre and millimetre fluxes.

A degeneracy between the inner radius and minimum grain size can still exist: in this case the σ-contours plots would represent only a local minimum in the parameter space, instead of the absolute solution. Only a resolved image of the entire grain population which delineates the inner radius of the disc will allow us to break the degeneracy between smallest grain size present in the disc and inner radius.

We now discuss how well constrained the fixed model parameters are (i.e. $R_{\rm OUT}$, $a_{\rm max}$, dust composition and size distribution) and in particular if and how they can alter our conclusions about $M_{\rm dust}$, $R_{\rm in}$ and $a_{\rm min}$. We are not going to further discuss the cases of HD 61005 and HD 191089 because our modelling was not significant at all, nor the case of HD 107146 because the assumption on the outer radius is supported by millimetre resolved images (Corder et al. 2009).

– The *outer radius* was assumed to be 150 AU. While in the case of HD107146 such an assumption is supported by resolved millimetre images, in the other cases, we need to investigate the robustness of our model results. While the most distant objects of the Kuiper belt have been observed up to 150 AU from the Sun (e.g. Gladman et al. 2002), the edge of the Kuiper belt is commonly considered close to the 2:1 resonance with Neptune at about 50 AU from the Sun (e.g. Trujillo & Brown 2001). There is also no reason why all discs would be expected to have the same outer edge. For these reasons we use five different outer radii (1000, 500, 300, 100 and 50 AU, or 60 AU when the fitting routine was not able to find any reasonable inner radius smaller than 50 AU), leaving free the dust mass ($M_{\rm dust}$), the inner radius ($R_{\rm in}$) and the minimum grain size $a_{\rm min}$. The results are summarised in Table 5. We notice that, in the case of HD 104860 and HD 8907, changing the outer radius from 500 to 50 AU affects only the dust mass. In the case of HD 377 fixing the outer radius to 100 and 50 AU the model fitting is no longer satisfactory, while we find a better result increasing the outer

Table 5. Model results leaving as free parameters using $M_{\rm dust}/M_{\oplus}$, $R_{\rm in}$ and $a_{\rm min}$ for 6 different outer radii: 1000, 500, 300, 150, 100 and 50 AU.

			HD 104860			
$R_{\rm OUT}$	1000 AU	500 AU	300 AU	150 AU	100 AU	50 AU
$M_{\rm dust}/M_{\oplus}$	5.843 ± 0.652	2.930 ± 0.245	1.774 0.133	0.082 ± 0.007	0.053 ± 0.005	0.039 ± 0.004
$R_{\rm in}$ [AU]	185 ± 23	20.3 ± 7.8	20 ± 7	21 ± 5	22 ± 2	30 ± 3
$a_{\rm min}$ [μm]	0.07 ± 0.03	4.5 ± 0.9	6 ± 2	8 ± 5	11 ± 2	21 ± 4
$\chi^2_{\rm red.}$	6.1	7.0	4.1	2.6	2.7	3.0
			HD 8907			
$R_{\rm OUT}$	1000 AU	500 AU	300 AU	150 AU	100 AU	60 AU
$M_{\rm dust}/M_{\oplus}$	3.097 ± 184	1.614 ± 0.099	0.931 ± 0.050	0.040 ± 0.005	0.024 ± 0.002	0.017 ± 0.003
$R_{\rm in}$ [AU]	89 ± 14	29 ± 14	19.4 ± 5.4	27 ± 17	27 ± 7	41 ± 15
$a_{\rm min}$ [μm]	0.5 ± 0.08	3.1 ± 0.8	5.6 ± 1.1	6 ± 2	8 ± 2	7.7 ± 2.6
$\chi^2_{\rm red.}$	22.8	17.8	9.2	4.3	3.6	3.5
			HD 377			
$R_{\rm OUT}$	1000 AU	500 AU	300 AU	150 AU	100 AU	60 AU
$M_{\rm dust}/M_{\oplus}$	3.655 ± 0.507	2.649 ± 0.322	1.339 ± 0.367	0.058 ± 0.013	0.034 ± 0.006	0.039 ± 0.012
$R_{\rm in}$ [AU]	70 ± 12	4.6 ± 1.1	4.6 ± 0.65	6.1 ± 0.8	38 ± 8	51 ± 8
$a_{\rm min}$ [μm]	0.02 ± 0.001	6.5 ± 1.5	9.1 ± 3.5	14 ± 5	14 ± 4	38 ± 20
$\chi^2_{\rm red.}$	8.6	7.7	4.6	5.0	395.	395.

radius up to 500 AU (see different $\chi^2_{\rm red.}$ in Table 5). The minimum grain size remains at least one order of magnitude bigger than the blowout size, despite the case of an outer radius of 1000 AU where it becomes of the same order of magnitude or smaller than the blowout size.

– The *maximum grain size* has been fixed to 3 mm; despite the fact that a collisional cascade generates a distribution of grain size which does not stop at the millimetre size, we include in our model the maximum particle size which contributes significantly to the emission which we detect during our observations. We remind the reader that the mass derived by our model represents the mass of the grains smaller than 3 mm present in the disc and that increasing the maximum grain size would increase the disc mass.
– The dust has been assumed to be made up of *astronomical silicate*; this is expected to be the main component in protoplanetary discs (Pollack et al. 1994). Although a different composition of the dust can be present in the disc, Spitzer infrared spectroscopic observations do not allow us to constrain the material properties due to the lack of diagnostic features, caused by large grain sizes (see the IRS spectra overplotted in the SEDs, Figs. 2–7). A different dust composition would change the blow-out size as well as the minimum grain size present in the disk computed by our model. A detailed investigation of different dust compositions is beyond the goal of this paper.
– We finally recall that a more realistic *grain size distribution* can also affect our modelling results. Departures from the canonical size distribution we assumed, have been highlighted by collisional evolution studies of spatially resolved debris disks (e.g. Thébault & Augereau 2007).

Despite previously discussed degeneracies, the objects HD 104860, HD 8907 and HD 107146 show the inner part of their discs cleared from small micron-sized dust grains because of the lack of near/mid-infrared emission (Wolf & Hillenbrand 2003). These inner holes can be maintained by the presence of a planet-sized body (Roques et al. 1994), which avoids the filling of the central cavity by Poynting-Robertson drag.

5. Summary and conclusions

We have carried out two deep surveys at 350 μm and 1.2 mm of circumstellar discs around solar-type stars at ages between 3 Myr and 3 Gyr. These new observations are an order of magnitude more sensitive to dust emission than previous observations of C05. The dust disc masses have been computed from the millimetre emission, where the discs are assumed to be optically thin. A survival analysis of the dust disc masses as a function of time has been carried out of systems older than 20 Myr, including the dust mass upper limits. The spectral energy distributions of the debris discs detected by our sub-millimetre and millimetre surveys have been modelled. We draw the following main conclusions from our work:

1. The *Kendall's tau correlation* yields a probability of 76% that the mass of debris discs and their age are correlated. Similarly, the three different *two-sample tests* gives a probability between 70 and 83% that younger and older debris systems belong to different parent populations in terms of dust mass. Our result on the relation between dust mass and age is limited by the sensitivity of our millimetre survey. Deeper millimetre observations are needed to confirm the evolution of debris material around solar-like stars.
2. The spectral energy distributions of the debris discs detected at 350 μm and/or 1.2 mm were modelled. We found a degeneracy in the best fit parameters which will only be broken with high-resolution images which resolve the entire disc. Nevertheless, this approach allows us to identify debris discs with an inner region that has been evacuated from small micron-sized dust grains.
3. In the case of the detected debris discs, the comparison between collision and Poynting-Robertson timescales suggests that the debris discs are collision dominated.

Acknowledgements. All the authors wish to thank the entire FEPS team for their work. V.R. thanks A. Sicilia-Aguilar for helpful discussions on the IRAM data reduction, E. Feigelson for his suggestions about the survival analysis, L. Hillenbrand for some details about the stellar ages, S. J. Kim for her suggestions about the FEPS sample, A. Pasquali and A. Martinez-Sansigre for reading the manuscript. S.W. was supported at the MPIA by the German Research Foundation (DFG) through the Emmy Noether grant WO 857/ 2. J.R. wishes

to thank Jesús Falcón-Barroso for a helpful discussion on how to project 3-d isosurfaces to lower dimensions. M.R.M. thanks support provided through the LAPLACE node of the NASA Astrobiology Institute. Research at the Caltech Submillimetre Observatory is supported by grant AST-0540882 from the National Science Foundation.

References

Andrews, S. M., & Williams, J. P. 2005, ApJ, 631, 1134
Andrews, S. M., & Williams, J. P. 2007, ApJ, 659, 705
Ardila, D. R., Golimowski, D. A., Krist, J. E., et al. 2004, ApJ, 617, L147
Backman, D. 2004, in Debris Disks and the Formation of Planets, ed. L. Caroff, et al. (San Francisco: ASP), ASP Conf. Ser., 324, 9
Backman, D. E., & Paresce, F. 1993, Protostars and Planets III, 1253
Beckwith, S. V. W., Sargent, A. I., Chini, R. S., & Güsten, R. 1990, AJ, 99, 924
Beckwith, S. V. W., Henning, T., & Nakagawa, Y. 2000, Protostars and Planets IV, ed. V. Mannings, A. P. Boss, & S. S. Russell, 533
Bevington, P. R. 1969, Data Reduction and Error Analysis for the Physical Sciences (New York: McGraw-Hill), 1
Bottke, W. F., Durda, D. D., Nesvorný, D., et al. 2005, Icarus, 179, 63
Brown, B. W. M., Hollander, M., & Korwar, R. M. 1974, Reliability and Biometry, ed. F. Proschan, & R. J. Serfling (Philadelphia: SIAM), 327
Buckley, J., & James, I. 1979, Biometrika, 66, 429
Burns, J. A., Lamy, P. L., & Soter, S. 1979, Icarus, 40, 1
Calvet, N., D'Alessio, P., Watson, D. M., et al. 2005, ApJ, 630, L185
Carpenter, J. M., Wolf, S., Schreyer, K., Launhardt, R., & Henning, T. 2005, AJ, 129, 1049
Carpenter, J. M., Mamajek, E. E., Hillenbrand, L. A., & Meyer, M. R. 2006, ApJ, 651, L49
Carpenter, J. M., Bouwman, J., Mamajek, E. E., et al. 2008, [arXiv:0810.1003]
Chen, C. H., Jura, M., Gordon, K. D., & Blaylock, M. 2005, ApJ, 623, 493
Corder, S. A., Carpenter, J. M., Sargent, A. I., et al. 2009, ApJ, 690, L65
Currie, T., Kenyon, S. J., Rieke, G., Balog, Z., & Bromley, B. C. 2007, ApJ, 663, L105
Cutri, R. M., et al. 2003, The IRSA 2MASS All-Sky Point Source Catalog, NASA/IPAC Infrared Science Archive, http://irsa.ipac.caltech.edu/applications/Gator/
de Zeeuw, P. T., Hoogerwerf, R., de Bruijne, J. H. J., Brown, A. G. A., & Blaauw, A. 1999, AJ, 117, 354
Dominik, C., & Decin, G. 2003, ApJ, 598, 626
Decin, G., Dominik, C., Waters, L. B. F. M., & Waelkens, C. 2003, ApJ, 598, 636
Draine, B. T., & Lee, H. M. 1984, ApJ, 285, 89
Feigelson, E. D., & Nelson, P. I. 1985, ApJ, 293, 192
Franco, J., Tenorio-Tagle, G., & Bodenheimer, P. 1990, ApJ, 349, 126
Ghez, A. M., Neugebauer, G., & Matthews, K. 1993, AJ, 106, 2005
Gladman, B., Holman, M., Grav, T., et al. 2002, Icarus, 157, 269
Habing, H. J., Dominik, C., Jourdain de Muizon, M., et al. 2001, A&A, 365, 545
Haisch, K. E., Jr., Lada, E. A., & Lada, C. J. 2001, ApJ, 553, L153
Handler, G. 1999, MNRAS, 309, L19
Hartmann, W. K., Ryder, G., Dones, L., & Grinspoon, D. 2000, Origin of the earth and moon, ed. R. M. Canup, K. Righter and 69 collaborating authors (Tucson: University of Arizona Press), 493
Helou, G., & Walker, D. W. 1988, Infrared astronomical satellite IRAS catalogues and atlases, 7, 1
Henning Th. 2008, Phys. Scr. T, 130, 014019
Henning, Th., & Stognienko, R. 1996, A&A, 311, 291
Hillenbrand. L. A. 2005, [arXiv:astroph/0511083]
Hillenbrand, L. A., Carpenter, J. M., Kim, J. S., et al. 2008, ApJ, 677, 630
Hines, D. C., Schneider G., Hollenbach D., et al. S. 2007, ApJ, 671, 165
Isobe, T., Feigelson, E. D., & Nelson, P. I. 1986, ApJ, 306, 490
Johansen, A., Oishi, J. S., Low, M.-M. M., et al. 2007, Nature, 448, 1022
Kenyon, S. J., & Bromley, B. C. 2001, AJ, 121, 538
Kenyon, S. J., & Bromley, B. C. 2002, AJ, 123, 1757
Kenyon, S. J., & Bromley, B. C. 2002, ApJ, 577, L35
Kenyon, S. J., & Bromley, B. C. 2004, AJ, 127, 513
Kenyon, S. J., & Bromley, B. C. 2004, ApJ, 602, L133
Kenyon, S. J., & Hartmann, L. 1995, ApJS, 101, 117
Kim, J. S., Hines, D.C., Backman, D. E., et al. 2005, ApJ, 632, 659
Koen, C., & Eyer, L. 2002, VizieR Online Data Catalog, 733, 10045
Lavalley, M., Isobe, T., & Feigelson, E. 1992, Astronomical Data Analysis Software and Systems I, ed. D. M. Worrall, C. Biemesderfer, & J. Barnes (San Francisco: ASP), 245
Lawson, W. A., Lyo, A.-R., & Muzerolle, J. 2004, MNRAS, 351, L39
Levison, H. F., Morbidelli, A., Gomes, R., & Backman, D. 2007, Protostars and Planets V, 669
Liu, M. C., Matthews, B. C., Williams, J. P., & Kalas, P. G. 2004, ApJ, 608, 526
Löhne, T., Krivov, A. V., & Rodmann, J. 2008, ApJ, 673, 1123
Mamajek, E. E., Meyer, M. R., Hinz, P. M., et al. 2004, ApJ, 612, 496
Mamajek, E. E., & Hillenbrand, L. A. 2008, ArXiv e-prints, 807, [arXiv:0807.1686]
Meyer, M. R., Hillenbrand, L. A., Backman, D., et al. 2006, PASP, 118, 1690
Meyer, M. R., Backman, D. E., Weinberger, A. J., & Wyatt, M. C. 2007, Protostars and Planets V, ed. B. Reipurth, D. Jewitt, & K. Keil (Tucson: University of Arizona Press), 951, 573
Meyer, M. R., Carpenter, J. M., Mamajek, E. E., et al. 2008, ApJ, 673, L181
Moór, A., Ábrahám, P., Derekas, A., et al. 2006, ApJ, 644, 525
Najita, J., & Williams, J. P. 2005, ApJ, 635, 625
Natta, A., Testi, L., Neri, R., Shepherd, D. S., & Wilner, D. J. 2004, A&A, 416, 179
Natta, A., Testi, L., Calvet, N., et al. 2007, Protostars and Planets V, ed. B. Reipurth, D. Jewitt, & K. Keil (Tucson: University of Arizona Press), 767
Nordström, B., Mayor, M., Andersen, J., et al. 2004, A&A, 418, 989
Pan, X., Shao, M., & Kulkarni, S. R. 2004, Nature, 427, 326
Pascucci, I., Gorti, U., Hollenbach, D., et al. 2006, ApJ, 651, 1177
Perryman, M. A. C., Lindegren, L., Kovalevsky, J., et al. 1997, A&A, 323, L49
Pinsonneault, M. H., Stauffer, J., Soderblom, D. R., King, J. R., & Hanson, R. B. 1998, ApJ, 504, 170
Pollack, J. B., Hollenbach, D., Beckwith, S., et al. 1994, ApJ, 421, 615
Prato, L. 2007, ApJ, 657, 338
Preibisch, T., Guenther, E., Zinnecker, H., et al. 1998, A&A, 333, 619
Preibisch, T., Brown, A. G. A., Bridges, T., Guenther, E., & Zinnecker, H. 2002, AJ, 124, 404
Press, W. H., Flannery, B. P., Teukolsky, S. A., & Vetterling, W. T. 1992, Numerical Recipes in C, 2nd edition (Cambridge University Press), Sect. 15.6
Rodmann, J., Henning, T., Chandler, C. J., Mundy, L. G., & Wilner, D. J. 2006, A&A, 446, 211
Roques, F., Scholl, H., Sicardy, B., & Smith, B. A. 1994, Icarus, 108, 37
Silverstone, M. D., Hines, D. C., Schneider, G., et al. 2006, ApJ, 650, 414
Smith, B. A., Becklin, E. E., Schneider, G., et al. 1999, ApJ, 513, L127
Setiawan, J., et al. 2008, Precision Spectroscopy in Astrophysics, 201
Silverstone, M. D. 2000, Ph.D. Thesis
Silverstone, M. D., Meyer, M. R., Mamajek, E. E., et al. 2006, ApJ, 639, 1138
Spangler, C., Sargent, A. I., Silverstone, M. D., Becklin, E. E., & Zuckerman, B. 2001, ApJ, 555, 932
Benedict, G. F., Nelan, E., Soderblom, D. R., et al. 2004, 36, 735
Song, I., Zuckerman, B., Weinberger, A. J., & Becklin, E. E. 2005, Nature, 436, 363
Strom, S. E., Edwards, S., & Skrutskie, M. F. 1993, Protostars and Planets III, 837
Rieke, G. H., Stransberry, J. A., Su, K. Y. L., et al. 2006, ApJ, 653, 675
Thébault, P., & Augereau, J.-C. 2007, A&A, 472, 169
Trujillo, C. A., & Brown, M. E. 2001, ApJ, 554, L95
Weingartner, J. C., & Draine, B. T. 2001, ApJ, 548, 296
Wichmann, R., Schmitt, J. H. M. M., & Hubrig, S. 2003, A&A, 399, 983
Williams, J. P., & Andrews, S. M. 2006, ApJ, 653, 1480
Williams, J. P., Najita, J., Liu, M. C., et al. 2004, ApJ, 604, 414
Wolf, S., & Hillenbrand, L. A. 2003, ApJ, 596, 603
Wright, J. T., Marcy, G. W., Butler, R. P., & Vogt, S. S. 2004, ApJS, 152, 261
Wyatt, M. C. 2005, A&A, 433, 1007
Wyatt, M. C., Dermott, S. F., Telesco, C. M., et al. 1999, ApJ, 527, 918
Wyatt, M. C., Dent, W. R. F., & Greaves, J. S. 2003, MNRAS, 342, 876
Wyatt, M. C., Smith, R., Greaves, J. S., et al. 2007a, ApJ, 658, 569
Wyatt, M. C., Smith, R., Su, K. Y. L., et al. 2007b, ApJ, 663, 365
Zacharias, N., Urban, S. E., Zacharias, M. I., et al. 2004, AJ, 127, 3043
Zuckerman, B., & Becklin, E. E. 1993, ApJ, 414, 793
Zuckerman, B., & Song, I. 2004a, ApJ, 603, 738
Zuckerman, B., & Song, I. 2004b, ARA&A, 42, 685
Zwahlen, N., North, P., Debernardi, Y., et al. 2004, A&A, 425, L45